Detection and Monitoring of Fatigue damage in SMCR26 Specimens using Spate, for a Constant Mean Stress – A Qualitative Approach

Maina Maringa

Department of Mechanical Engineering, Jomo Kenyatta University of Agriculture and Technology, P. O. Box 62000, Nairobi, KENYA Email: maina_wamaringa@yahoo.com

ABSTRACT

The primary aim of the work presented here was to establish the use of thermoelastic measurements in detecting the presence of damage and its subsequent accumulation in sheet moulding compound (SMCR26). To this end, several dog bone shaped specimens of SMCR26 were cycled at a constant mean stress of 38.87 MPa and at varying stress amplitudes, the latter in order to investigate any dependencies on stress amplitude. Surface scans were taken from each specimen at various stages in their load history using the Stress Pattern Analysis by Thermal Emission (SPATE) measurement equipment. The first scan obtained from each specimen was used to determine its initial state of damage, while subsequent scans were used to monitor the accumulation of damage. The thermoelastic signal in the initial and subsequent scans exhibited different magnitudes and distribution for the different specimens, which denoted heterogeneity of the SMCR26 specimens and of the occurrence and accumulation of damage. This was in sharp contrast to the uniform thermoelastic signal that is emitted from the surfaces of cycled, undamaged homogeneous materials. The absence of any apparent relationship between the stress amplitude and the accumulation of damage in the tested specimens was thought to be a result of the in-homogeneity inherent in SMCR26, and of the heterogeneous nature of the accumulation of damage, rather than a limitation of the thermoelastic equipment used. The results obtained in this work demonstrated SPATE to be a fast and useful means of detecting the presence of damage and of monitoring its accumulation.

Key Words: Sheet Moulding Compound (SMC), Fatigue, Damage

1.0 NOMENCLATURE

s - Stress

s_m - Principle stress sum $(\sigma_{11} + \sigma_{22} + \sigma_{33})$

σ - Direct stress

σ_{11} - Principal stress in the principle 11-direction

σ_{22} - Principal stress in the principle 22-direction

σ_{33} - Principal stress in the principle 33-direction

σ_{12} - Shear stress in the 12-pane

τ - Shear stress

μ - Lame constant

ν - Poisson's ratio

E - Elastic modulus

N - Newtons

MPa- Mega Pascals

GPa- Giga Pascals

K, k - Thermoelastic constant

K_m - Thermoelastic parameter

α - Coefficient of linear thermal expansion

α_{11} - Coefficient of linear thermal expansion in the principle 11-direction

α_{22} - Coefficient of linear thermal expansion in the principle 11-direction

α_{12} - Coefficient of linear thermal expansion in the 12-plane

T - Temperature in degree Kelvin

θ', ΔT - Temperature change

C_p - Constant temperature heat capacity

C_v - Constant volume heat capacity

Δ - Change

ρ - Density

σ_o - Characteristic strength

2.0 INTRODUCTION

Amongst the various methods that are used to monitor the micro-mechanisms of fatigue damage in composites are the ultrasonic, acoustic laser testing and acoustic emission scanning techniques. The first two methods are normally used to observe de-lamination and the growth of impact damage, while the last method is used to detect fibre fracture and the growth of matrix cracks. Differences and changes in the character of the propagated signal are used to distinguish areas with damage from those without and to monitor its accumulation, respectively, in the first two methods. The last method uses the different types of recorded events and their different intensities to identify the presence of damage and to monitor its accumulation. Because all these factors are dependent on the condition of the material tested, the heterogeneous nature and complex interaction of the various failure mechanisms in composites, particularly randomly oriented short fibre reinforced composites, limit the predictive use of these three methods. The area resolution of the three methods is limited by the size of probes used, as all require contact between the probes and the test material. Development in the use of ultrasonic non-contact [Khoury *et al* (1999)] and phased array [Lonsdale and Meyer (2000)] methods, despite the complex analytical techniques involved in them is likely to increase application of ultrasonic testing methods in the detection and monitoring of damage. In contrast to these three methods, thermoelastic measurement techniques are non-contact and can be used to provide point, line and area data, in addition to which, the size of the area for which data is needed can be specified and varied as required. By obtaining special attachments, the spatial resolution of the thermoelastic measurements equipment SPATE, can be raised from the standard 500 μm to 150 μm, thus giving a significant increase in the level of detail obtained from the scanned surfaces [Everett *et al* (1990)]. The accuracy of thermoelastic data obtained can also be enhanced by changing the size of the scanned spots, increasing the number of repeat scans per spot, as well as the dwell time on each scanned spot and also by increasing the overlap between scanned areas. Thermoelastic measurement techniques clearly do have an advantage over the other three methods.

One of the aims of the research reported here was to investigate use of the thermoelastic measurement equipment SPATE in detecting the presence of damage and

monitoring its accumulation in SMCR26 specimens. This being the first phase of a broader project dealing with the accumulation of damage generally, the research was initially restricted to the qualitative study of the accumulation of damage in cycled SMCR26 specimens. The study was expected to establish the manner in which damage occurred in SMCR26 specimens and its dependence on the nature of the material, whether homogeneous or heterogeneous. The results obtained were also expected to give an indication of the manner in which damage grew in intensity and spread over the surface of the cycled specimens.

In order to achieve these aims a test procedure in which different test specimens were exposed to tension-tension cycling, at the same means stress and different stress amplitudes, with SPATE scans being obtained at specific periods throughout the test life was adopted. Subsequent analysis of the SPATE scans obtained was to be carried out in order to determine the magnitude and distribution of the thermoelastic signals obtained and the manner in which they varied with time. It was anticipated that this would provide a basis for determining the level of damage, growth in its intensity and spread over the surface of the cycled specimens. It must be emphasised here that because a qualitative rather than a quantitative method of analysis was adopted in the present work, the analysis presented in this paper is restricting visual examination of the obtained SPATE scans. Further and more detailed quantitative analysis formed the subject of further work carried out under the broader general aims [Maringa (2002)] and will be reported at a later date.

Early research on the thermoelastic effect can be traced to the work of Gough in 1805, as reported by Harwood et al (1991a). Weber (1830) observed that the frequency of a vibrating wire under a stress increase was somewhat higher than the expected value and that this was due to a thermal effect. This effect was later summarised in what is now known as the thermoelastic equation, given here as Equation 1, by Thomson (1851) in which he showed the generated heat Q to be a direct function of the stress change $\Delta\sigma$ in a material at the temperature T.

$$Q = -kT\Delta\sigma \quad \text{..... 1}$$

Commenting on the effect of compressive and tensile loads on vulcanised Indian rubber and metallic pillars, Joule (1857), observed that the temperature of the two materials increased or decreased as a result of imposed compressive or tensile loads, respectively. Rocca and Bever (1950) noted that those materials, which had positive or negative coefficients of thermal expansion, when exposed to tensile or compressive loads, experienced respective decreases and increases in temperature. The authors also noted that these changes in temperature reversed whenever the sign of the coefficient of thermal expansion changed and that plastic deformation in the materials gave rise to the generation of heat in the active slip zones, with a resulting reversal in the direction of temperature change. This reversal was observed to be gradual for non-annealed copper and nickel and sharp for carbon steels.

By defining the deviatoric stress component such that the hydrostatic stress was equal to zero, Dillon Jr. (1963) developed terms for both the dissipative deformation variable and the state deformation variable. These two terms were then applied to the energy equation, assuming conservation of energy, to develop a coupled thermoplastic equation of heat conduction, for cycled aluminium tubes. In a later publication, Dillon Jr. (1966) observed that the theory of thermoelasticity represented temperature changes in cycled materials, which arose from the changing frequencies at which its atoms vibrated, as a result of changing inter-atomic distances. He noted that the "stored energy of cold work" in metals was in the range of 10%, being the difference between the plastic work done on a material and the resulting heat generated by the material. Copper tubes that were cycled in torsion over a full cycle showed the difference to remain positive over most of the cycle, though changing sign at certain instances in the cycle. Based on idealised experimental processes and without explicitly defining the dissipation deformation variables, as was the case in his previous work mentioned above, he then went on to develop a general and more explicit equation of coupled thermoplasticity.

Stanley and Chan (1988) extended the thermoelastic equation, rewritten in the format shown in Equation 2, to orthotropic materials thus giving rise to Equation 3

$$Q = -kT\Delta\sigma = \left(T/\rho C_p\right)\Delta\sigma \quad \ldots\ldots 2$$

$$\Delta T = \left(T/\rho C_p\right)\left(\alpha_{ii}\Delta\sigma_{jj}\right) \quad \ldots\ldots 3$$

Equation 3 for a 2-D system in the 12-plane was then shown by the two authors to reduce to;

$$\Delta T = (T/\rho C_p)(\alpha_{11}\Delta\sigma_{11} + \alpha_{22}\Delta\sigma_{22} + \alpha_{12}\Delta\sigma_{12}) \quad \ldots\ldots 4$$

They observed that the last term in the above equation implied that orthotropic materials would emit a non-zero thermoelastic signal under pure shear loading, unlike isotropic materials. The work of Dillon Jr. (1963, 1966) mentioned above is relevant, for cases of pure shear loading of isotropic materials. The mean stress dependency of the thermoelastic signal was illustrated experimentally in the separate works of Machin *et al* (1987a, 1987b) and Dunn *et al* (1989) and rigorous theoretical proof based on the free energy approach presented by Wong *et al* (1987). In their work, Wong *et al* (1987) showed that what had so far been referred to as the thermoelastic constant $(K = \alpha/\rho C_p)$, was indeed a parameter (K_m) represented by the equation;

$$K_m = (\alpha/\rho C_e)(\alpha - (\nu/E^2)(\partial E/\partial T)s_m) \quad \ldots\ldots 5$$

Based on this expression for the thermoelastic parameter, they then presented the following modified thermoelastic equation for a sinusoidal oscillating load defined by the expressions $\sigma = \sigma_m + \Delta\sigma \sin\omega t$ as;

$$\rho_o C_e(\Delta T/T_o) = -(\alpha - (\nu/E^2)(\partial E/\partial T)s_m)\Delta s \sin\omega t + (1/4E^2)(\partial E/\partial T)(\Delta s)^2(1 - \cos 2\omega t) \quad \ldots\ldots 6$$

3.0 INFRARED RADIOMETRIC EQUIPMENT

Experimental non-contacting infrared radiometry and it use in determining the dynamic stress in a body, was first illustrated by Belgen (1967), who developed the linear equation $\theta' = K_m T s'$ relating the difference (θ') between the instantaneous temperature and the average temperature, the average temperature (T) and the stress (s'). He defined the parameter K_m as a constant dependent on the constant pressure heat capacity (C_p), thermal expansion coefficient, (α) the elastic modulus (E), density (ρ), Poisson's ratio (ν) and the Lame constant (μ) and recommended the method for use in the rapid acquisition of stress data at elevated temperature testing. Despite this obvious application, thermoelastic stress analysis has had to await development in radiometric signal acquisition and processing technology, in the 1970's and 1980's and the eventual manufacture of the first commercial single detector thermal imaging equipment SPATE

8000 in 1982 [Harwood et al (1991a)]. Subsequent improvement in the signal acquisition, processing and display abilities led to the manufacture of the single detector SPATE series 9000 and 4000 upgrades.

Enke (1989) observed that an ideal photon detector was equally responsive to all photons having energies greater than the band-gap energy, which for the SPATE photodiode implies all wavelengths less than 12.4 μm. The SPATE head consists of a single mercury-cadmium-telluride photodiode detector onto which infrared energy from a specific point on a loaded specimen is focused by a germanium lens. The lens receives the energy from a set of motorised horizontal and vertical mirrors that are inside the detector housing. The radiated energy goes through a beam splitter that divides the energy beam into infrared and visible rays. The infrared ray is then led to the detector while the latter goes to an eyepiece that is used to manually focus the detector onto any desired spot on the specimen. The location of the scanned spot is set using a hand set, which is also used to define the limits of the scanned area.

During scanning, the motorised mirrors in a SPATE head are controlled by a processor based on set scan parameters, which define the dwell time per spot, the distance between scanned spots and the scanned area. Noise is filtered from the detected thermoelastic signal by a lock-in-amplifier using the load signal generator signal as a reference. Figure 1 shows an outline of the SPATE head and its auxiliary equipment after Boyce (1991).

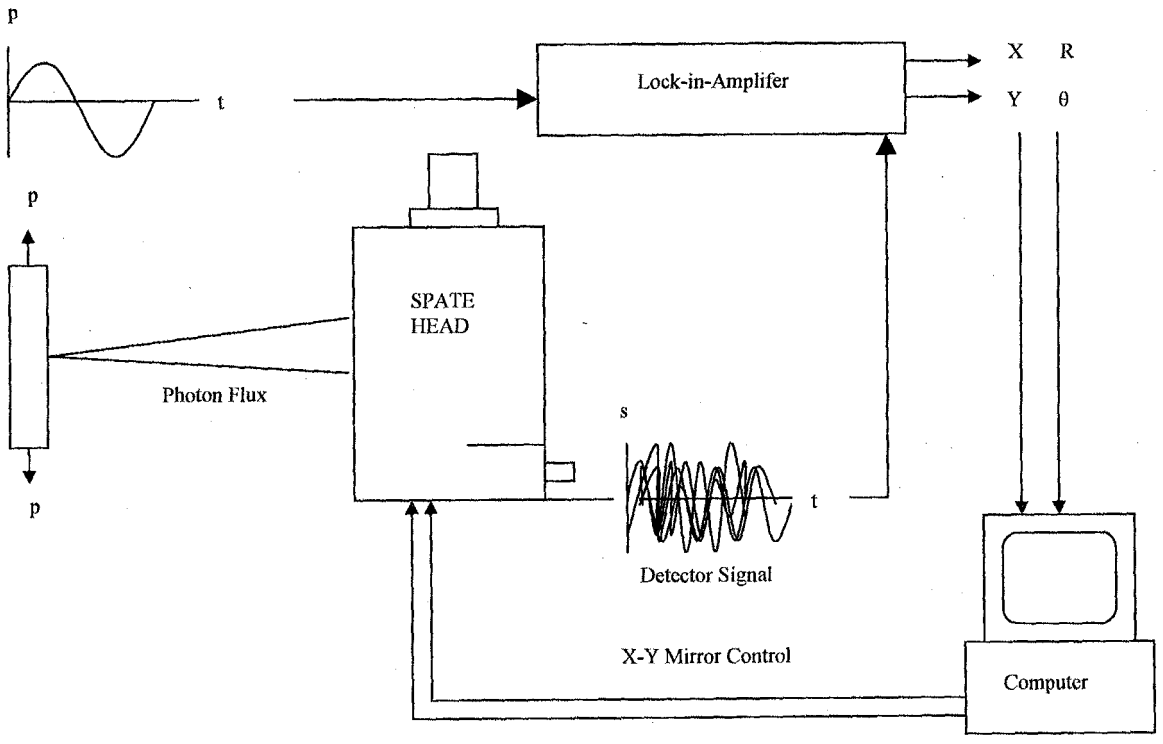

Figure 1: A Line Diagram Outline of the SPATE Head and it's Ancillary Equipment after Boyce (1991)

Harwood and Cummings (1991b) observed that a sinusoidal load signal was used because of the fact that noise segregation was most efficient when the required signal was at a fixed frequency. Better noise rejection and repeatability are obtained for higher dwell times as is provided for in the design of the lock-in–amplifier. The SPATE system processor is also used to convert the obtained scan data into a colour contour stress mapping and has programs that facilitate the storage and analysis of the converted stress mappings. SPATE is essentially a low frequency scanning system with best performance between 0.5 Hz and 25 Hz. Addition of a high frequency card into the correlator facilitates scanning at higher frequencies [Ometron (1987)]. The infrared resolution of SPATE varies between 0.5 mm - 5.0 mm square, for stand off distances between 250 mm and 4750 mm, respectively [Ometron (1987)]. Though spatial resolution enhancing attachments are known to improve the resolution of SPATE to 150 μm [Everett et al (1987)], none were available however, for use in the present work. Work carried out by Wang and Chim (1983) on SMCR50 showed the majority of visible fatigue damage cracks to be shorter than 1 mm in length. As SMCR26 and SMCR50 differ in composition

only in their respective reinforcing glass fibre contents of 26% and 50%, the character and dimensions of fatigue damage cracks in the two materials is expected to be the same. The small length of expected fatigue cracks meant that SPATE with its normal spatial resolution of 500 μm, could not be used to study the mechanisms of fatigue damage, but rather was restricted to the study macroscopic accumulation of fatigue damage.

The SPATE equipment is designed to give patterns of the sum of principal stress amplitudes based on the principles of linear elastic adiabatic thermoelasticity. The patterns are presented with a standard colour coding, running through from white, green, blue, black, brown, red, and orange to yellow, in increasing order of the obtained thermoelastic signal. The SPATE software has facilities for automatically centring the colour key. In an area scan whose principal stress sums range from positive to negative, white and yellow colours represent the highest negative and positive sums of the principal stress amplitudes, respectively. The intermediate stresses are then graded between these two extremes, thus facilitating easy identification of damage, its intensity and spread. A similar method is used to allocate colour contours using the same colour scheme, in situations where the stresses are all positive or negative [Ometron (1987)]. All the SPATE scans in this paper have been presented in grey scale, however, in order to minimise the cost of printing and that of making future reprints.

SPATE equipment has now been superseded by the array detector DELTA THERM 1300 & 1350, 1400 & 1450 and 1500 systems, which are more superior in terms of scanning speed and resolution. DELTA THERM consist of a lightweight, scan head that is less than 3.5kg in weight with 128 × 128, to 320 × 256 arrays of InSb detectors for the various models that are in the market. These include the open cycle DELTA THERM 1300 and 1400 series, with liquid nitrogen refill Dewar vessels that have hold-times of just over 50 hours. The closed cycle DELTA THERM 1350, 1450 and 1550 systems offering over 5000 hours of scanning before any refill of the coolant is required are yet another set of models. Real time imaging is facilitated by a digital processor, which handles over 1000 frames/second. The processor has DELTA VISION software installed in it for control of the equipment and the processing of the acquired data. The software runs within Windows 95 and Windows NT operating systems and requires a PC with the equivalent specifications of a Pentium II. A zoom lens allows monitoring of any areas

with notable activity and therefore makes the equipment very suitable for monitoring the accumulation of damage. The equipment comes with 25 mm, 50 mm and 100 mm lenses that facilitate resolutions down from the 150 microns obtained with single lenses to 15 microns, when a two-position zoom lens is used. It has a wide scanning frequency band, between 1 Hz and 100 Hz [Stress Photonics (2002)].

4.0 DAMAGE ACCUMULATION

The thermoelastic signal emanating from an isotropic homogenous material that is exposed to a uniform cyclic load is expected to be constant over its entire surface varying, as was noted by McKelvie and MacKenzie (1991), only in those cases where surface or internal stress concentrations exist. Progressive growth of internal flaws and defects give rise to a progressive increase in the magnitude of surface stresses and thus a progressive increase in the magnitude of the measured thermoelastic signal [Dulieu-Smith and Stanley (1996)]. This is not entirely surprising as degradation of material reduces its ability to carry load, thus leading to a transfer of stress to the undamaged sections along the same cross-section.

Damage in random short fibre reinforced composites accumulates in the form of cracks as a result of the combined occurrence of various failure mechanisms, including the growth of voids, matrix cracking, interfacial bond failure, fibre pullout, which give rise to a reduction in the stiffness and coefficient of linear thermal expansion [Mitrovic and Carman (1996)]. Examination of the thermoelastic equation shows that a reduction in the coefficient of thermal linear expansion will lead to a reduction in the thermoelastic signal. Further reduction in the magnitude of the signal arises from the fact that voids cannot carry stress and therefore cannot emit any stress related energy. The various heat generating failure mechanisms that are prevalent in areas of damage also give rise to a reduction in the magnitude of the measured signal and can lead to a reversal of the measured tensile-tensile cyclic test thermoelastic signal. These effects are in contrast with the effect of increasing magnitudes of the emmissivity of materials as a result of increasing crack lengths [Liao *et al* (1993)]. The SPATE users manuals show that SPATE surface temperature correction factor (R) varies with the surface temperature of the scanned surface [Ometron (1987)]. Changes in temperature due to the various heat

generating mechanisms prevailing during the accumulation of damage, will therefore require corrections to be made to the SPATE surface temperature correction factor (R) of the infrared detector. Clearly, therefore, the thermoelastic method does provide an indirect means of detecting the presence of damage and of monitoring its accumulation in composites. This is consistent with the observations made by Stinchcomb *et al* (1975), that the temperature distribution patterns of cycled materials conformed to the stress distribution patterns whose position and change in position reflected the location and spread of fatigue damage. Dulieu-Smith and Stanley (1996) noted that as a result of phase changes and reductions in the magnitude of the thermoelastic signal in areas with surface damage, the magnitude of the obtained signal could be used as a measure of the level of sustained damage. Potter and Wong (1994) made the conclusion, from the works of Van Hemelrijck *et al* (1990, 1991), that fretting, arising from the effects of hysteresis and/or de-lamination, led to the internal generation of heat in loaded composites.

Several thermoelastic damage models have been developed, defining damage parameters for use in the quantitative analysis of damage in composites [Dulieu-Smith and Stanley (1996), Jones *et al* (1989), Zhang and Sandor (1992a, 1992b)]. The models are however, all computationally demanding, particularly in cases where numerous damage sites occur, as was the case with the SMCR26 coupons that were tested in the present work. The results presented here only facilitate the qualitative analysis of damage as the development of alternative models that are less demanding computationally was considered beyond the scope of the present work.

The foregoing review shows that the presence of damage sites introduces stress concentration centres with resulting non-uniformity in the principal stress sums over the surface. The review also shows that the accumulation of damage, which is known in fibre reinforced composites to occur in the form of cracks, leads to a reduction in the magnitude of both the elastic modulus and the coefficient of thermal expansion at the damage sites. For surface sites of damage, a reduction in the magnitude of both the elastic modulus and the coefficient of thermal expansion produces a reduction in the magnitude of the thermoelastic signal. But for internal damage sites, the accumulation of damage give rise to an increase in the surface stress, which in turn produces a higher thermoelastic signal. Clearly, therefore, the variation in the magnitude and distribution of

the thermoelastic signal acts as a measure of the increase in the intensity of damage as well as its spread and can also be used to distinguish between the accumulation of surface and internal damage.

5.0 EXPERIMENTAL PROCEDURE

Sheet Moulding Compound (SMC) is a polyester compound comprised of randomly oriented short glass fibre, polyester resin and limestone filler. The different percentages of the constituents, length and predominant orientation of the reinforcing fibre, as well as the different ways in which they are produced distinguish different types of polyester compounds. SMCR26 for instance, is a randomly oriented short glass fibre reinforced polyester resin/limestone filler composites, with a fibre content by weight of 26%. Mixing in the production of SMC is only carried out during the formulation of the polyester/limestone matrix and not after the addition of the reinforcing glass fibre. DMC (Dough Moulding Compound), on the other hand, is comprised of randomly oriented short glass fibre (3 – 12mm) polyester resin/limestone filler, in which mixing is carried out after the addition of the reinforcing glass fibre. The reinforcing glass fibre in SMC is normally of length between 20mm and 50mm long and is added into the polyester resin, limestone filler matrix in weight fractions of 20%, 25%, 30% or 35%. The elastic modulus of polyester compounds lies between 8 GPa and 12 GPa. SMC composites have uniaxial and flexural strengths lying in the ranges 60 MPa to 90 MPa and 160 MPa to 190 MPa, respectively [Quinn (1989); Melby and Castro (1989); Whelan and Goff (1989)].

The formulation process of SMC involves the cutting of continuous long glass fibre strands on a Z-blade cutter, which then fall on a moving sheet of compounded polyester resin /limestone filler matrix that is carried on a thin sheet of polystyrene. The glass fibre, polyester resin/limestone filler composite is then passed under needling rollers in order to introduce planar homogeneity in it and to also ensure proper wetting of the reinforcing fibre. The glass fibre reinforced polyester resin is then stored below room temperature until needed for fabrication of components. When required, the SMC sheets are cut out into specified shapes and then placed into moulds with mould charge coverage of 50-90%. Two alternative routes are followed, either cold press moulding or hot press moulding. Cold press moulding is normally done with mould platen pressure of 120 KPa

and at room temperature, while hot press moulding is normally done at a pressure of 1 MPa and at temperatures between 100^0C-130^0C [Whelan and Goff (1989)].

Dog bone shaped specimens, such as the one shown in Fig. 2, were prepared and tested according to ASTM Standard E466 and BS 3518: Part 1 of 1993. Each specimen was mounted onto an Instron 8501 loading frame and then cycled according to the load schedule shown in Table 1, till fracture or up to a maximum of 10^6 cycles. The percentages in Table 1 are referred to the minimum uniaxial tensile strength σ_f of 73.74 MPa for SMCR27 [Dwyer et al (1993)]. The maximum stress σ_{max} in the table is defined as the sum of the mean stress σ_m and the stress amplitude σ_a. SMCR26 and SMCR27 differ in composition only in their respective reinforcing glass fibre contents of 26% and 27%. All test stresses were limited to between 5% and 95% of the minimum uniaxial tensile strength mentioned above, in order to ensure that overshoot of any imposed stresses did not create compressive stresses or cause tensile failure of the specimens, respectively. The applied stresses were all in excess of the yield stress of 12 MPa given by Dwyer *et al* (1993) for SMCR27 and the corresponding strains were all below the lowest fracture strain of 0.85% given by Garroch (1996) for SMCR26. SPATE scans were obtained from the gauge length area, in intervals of $n_1 \times 10^4$ cycles, $n_2 \times 10^5$ and $n_3 \times 10^6$ cycles, where n_1, n_2 and n_3 lay between 4 - 9, 1 – 9 and 1 - 2 respectively. Reference was made in this work to the values of strength for SMCR27 due to the absence of data for SMCR26. The 1% difference in the weight fraction of the two, SMCR27 and SMCR26, was considered so small as to cause insignificant differences in their respective mechanical properties, particularly given their statistical nature.

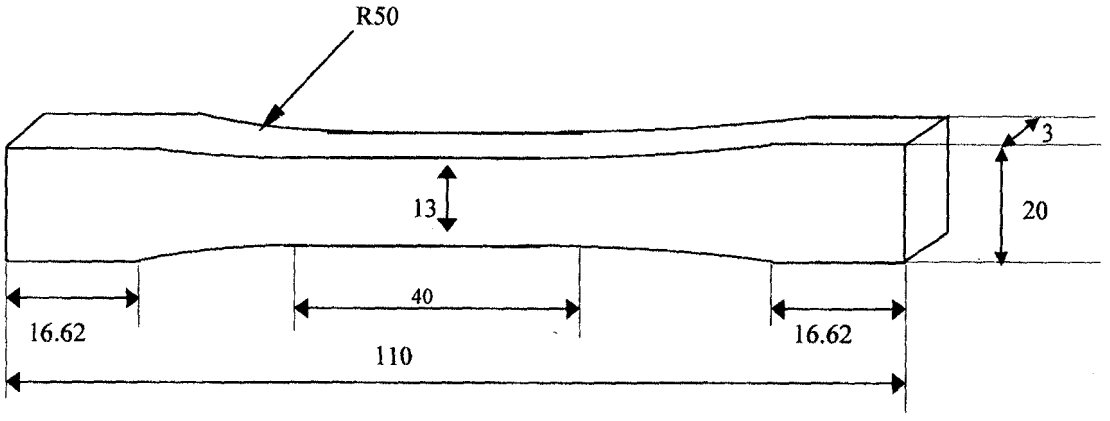

All dimensions in mm

Figure 2 Dog bone shaped specimen.

Table 1: Testing Schedule for Dog Bone Shaped SMCR26 Specimens

Specimen number	C4	A4	I3	I1F	I1R	I2	A2
Mean stress (MPa)	36.87	36.87	36.87	36.87	36.87	36.87	36.87
Stress amplitude (Mpa)	10.26	12.54	15.38	15.38	15.38	17.95	17.95
Maximum stress (Mpa)	47.13	49.41	52.25	52.25	52.25	54.82	54.82
σ_m/σ_f (%)	50	50	50	50	50	50	50
σ_{max}/σ_f (%)	64	67	71	71	71	74	74

The alphabetic letters and numbers in the designations of the specimens in this table, refer to the section on the central region of parent SMCR26 sheet, shown in Fig. 3, from which a respective specimen was obtained and the particular one of the five specimens cut out of every section. The specimens tested were randomly selected from the nine sections shown in Fig. 3. Before any tests were carried out, the width and thickness of a each dog bone specimen was determined at three points within the gauge section in order to obtain an average value of each specimen's gauge section cross sectional area. Two coatings of matt black were applied on each specimen and time intervals allowed for the each applied coating to dry. The SPATE equipment was calibrated by equating the thermoelastic signal obtained from the surface of a cycled specimen to a known value of planar stress, which was computed from the values of applied load amplitude and average

cross-sectional dimensions of the specimen. The calibration factor thus defined was used for all subsequent SPATE scans. While the heterogeneity of SMCR26 was expected to introduce some spatial variation in the SPATE signal obtained [Maringa (2002)], the results in the next section show this to have had little effect on the ability of the equipment to identify damage and to monitor its accumulation.

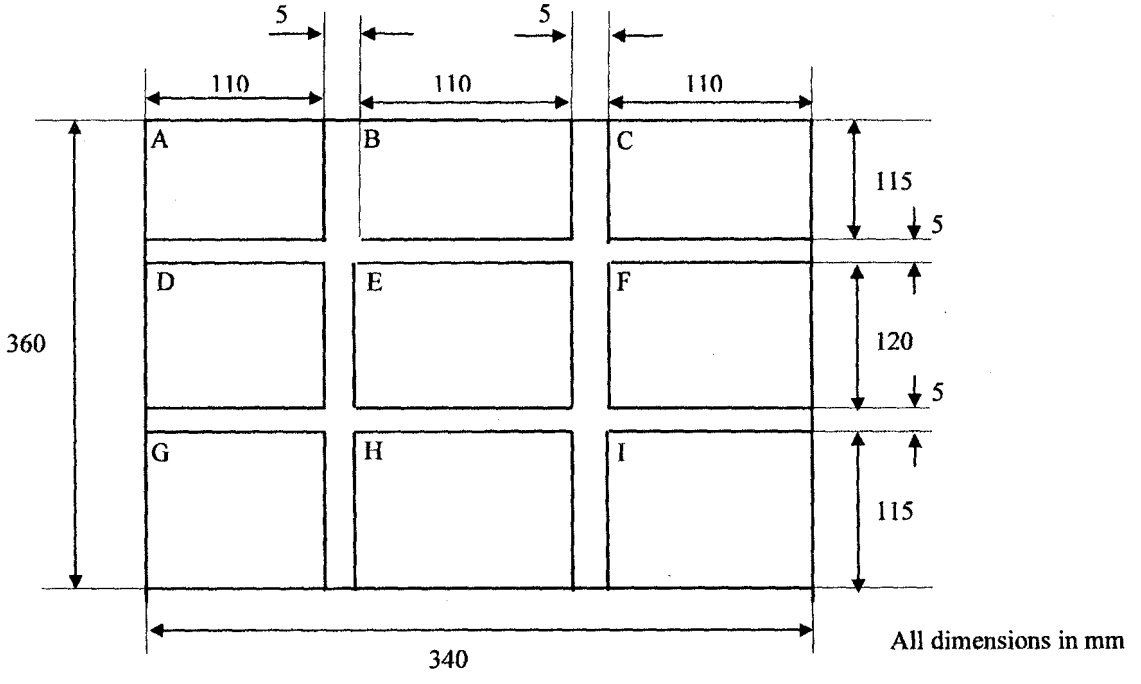

Figure 3:Test specimen cutting schedule from a SMCR26 parent sheet

All the SPATE scans were taken at ambient temperatures and at stand off distances of between 0.7 m and 0.9 m. In order to ensure adiabatic test conditions prevailed on the cycled specimens before the onset of damage, test frequencies of 10 Hz or 20 Hz were used. Garroch (1996) gave a minimum value of 6 Hz as being necessary to ensure adiabatic test conditions for SMCR26. In all 11, 15, 13, 6, 10 and 10 SPATE scans were obtained from specimens A4, I3, I2, A2, I1F and I1R, respectively. Though the analysis and discussion presented here is based on the complete set of scans for each specimen [Maringa (2002)], only the first and last scans that were obtained from each specimen are shown here in order to rationalise the length of the paper.

6.0 RESULTS AND ANALYSIS

In this and the next two sections, the thermoelastic signal is given units of MPa in all cases. This is a result of the calibration exercise carried out at the beginning of the experimental work in which the magnitude of the thermoelastic signal obtained was related to a known value of the planar stress sum $\Delta\sigma_{11} + \Delta\sigma_{22} = \Delta\sigma$ for a uniaxially loaded specimen.

A specific nomenclature has been adopted in this paper, which identifies the specimen number, the front (F) and/or rear (R) surfaces of the specimens that were scanned and the number of each scan. Thus, for example, G2F15 denotes the 15th scan of specimen G2, obtained from its front surface, and E3R2 stands for the 2nd scan of specimen E3 obtained from its rear surface. Unless otherwise stated the SPATE scans shown here were all taken from the central gauge section of each respective dog bone specimen. The SPATE scans presented here covered both the scanned specimen surface and the background surrounding the specimen. The background is distinguished from the specimen surface as the area with a uniform colour, surrounding a central region with varying colour contours, which represents the specimen surface. The absence of properly defined specimen edges in the SPATE scans shown here was probably a result of delamination at the edges.

The SPATE scans C4FR01 and A4R01 shown in Fig. 4 have been presented to illustrate the existence of initial surface and edge damage on the scanned specimens. Specimen A4 was loaded to mean, amplitude and maximum stresses of 36.87 MPa, 12.54 MPa and 49.41 MPa, respectively and the specimen was cycled at 20 Hz. The SPATE scans for specimen A4, two of which are shown in Fig. 5, exhibited both edge and surface sites of initial damage. The magnitude of the measured signal seen in the initial SPATE scan of specimen A4 was higher than the externally applied stress amplitude, over most of the scanned surface, which is an indication of widespread initial internal bulk damage. It is important to remember here that internal damage leads to a redistribution of stress, which in turn gives rise to an increase in the magnitude of stresses on the corresponding areas on the surface of the specimen and thus a higher thermoelastic signal. The increase in the severity of damage on the scanned surface of the specimen can be traced by a close examination of the magnitude of the SPATE signal at different times in the life cycle of

the specimen. The magnitudes of the SPATE signal on the specimen were seen to be predominantly below 20.62 MPa at 2.63×10^5 cycles, 14.70 MPa at 4.81×10^5 cycles, 6.19 MPa at 8.68×10^5 cycles and 5.00 MPa at 9.82×10^5 cycles. The fast change in the magnitude of the obtained signal from one that was initially greater than the imposed stress to one that was significantly less, points to a very rapid increase in the intensity of surface damage on the specimen, relative to the internal damage. The spread of damage on this specimen, seen from the reduction in the magnitude of the obtained signal over the scanned surface with time, was very extensive.

Specimen I3 was loaded at mean, amplitude and maximum stresses of 36.87 MPa, 15.38 MPa and 52.25 MPa, respectively and was cycles at 20 Hz. The initial SPATE scan for specimen I3, which was taken at 0.10×10^5 cycles, exhibited both edge and surface damage, with signal amplitudes that were below 11.98 MPa.

As can be seen in Fig. 6, damage in the specimen spread inwards from the edges. The amplitude of the thermoelastic signal, over most of the scanned surface, remained within the range 11.98 MPa to 6.03 MPa up until 3.77×10^5 cycles when the amplitude dropped down to the range 7.40 MPa to 6.52 MPa. This point marked the onset of the continuous decrease in the amplitude of the thermoelastic bulk signal. The amplitude of the thermoelastic signal eventually dropped down to the range 0.87 MPa to 0.74 MPa at 1.02×10^6 cycles. Initial damage on this specimen occurred on the surface/edge site near the bottom left edge and all around the specimen edge. While both sites had the same initial signal amplitude in the range 3.27 MPa to 1.05 MPa, the surface/edge site exhibited a more rapid decrease in the amplitude of the signal and thus a more rapid increase in the severity of damage. This was evident at the surface/edge site, which had a minimum thermoelastic signal amplitude that was in the range -6.51 MPa to -2.17 MPa at 1.76×10^5 cycles, at a time when the amplitude of the thermoelastic signal along the edges was in the range to 2.12 MPa to 8.51 MPa. A minimum amplitude of the thermoelastic signal along the edges of -0.78 MPa to -2.18 MPa was attained at 5.87×10^5 cycles. The negative signal amplitudes recorded from the surface of this specimen, were an indication of intense heat generation probably as a result of friction at the fibre/matrix interface.

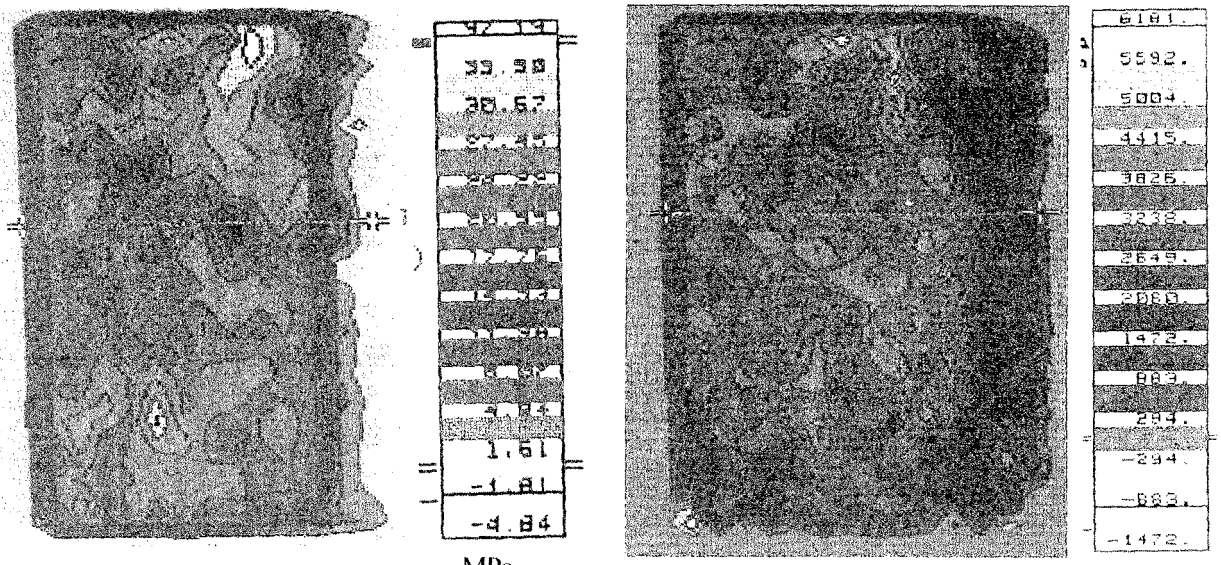

0.22×10^5 load cycles

9.82×10^5 load cycles

Figure 4: Initial edge and surface zones of stress reversal for damage load level cyclic loading of specimens C4 (left) and A4 (right)

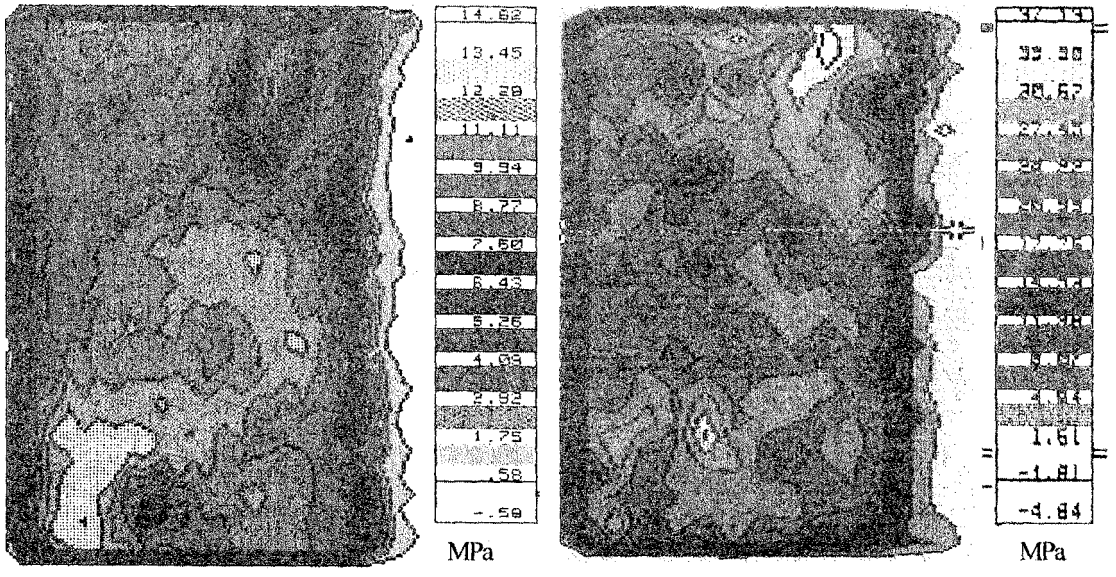

1.10×10^5 load cycles

0.22×10^5 load cycles

Figure 5: Initial SPATE scan A4F01 (left) and last SPATE scan A4F11 (right) both showing the presence of damage

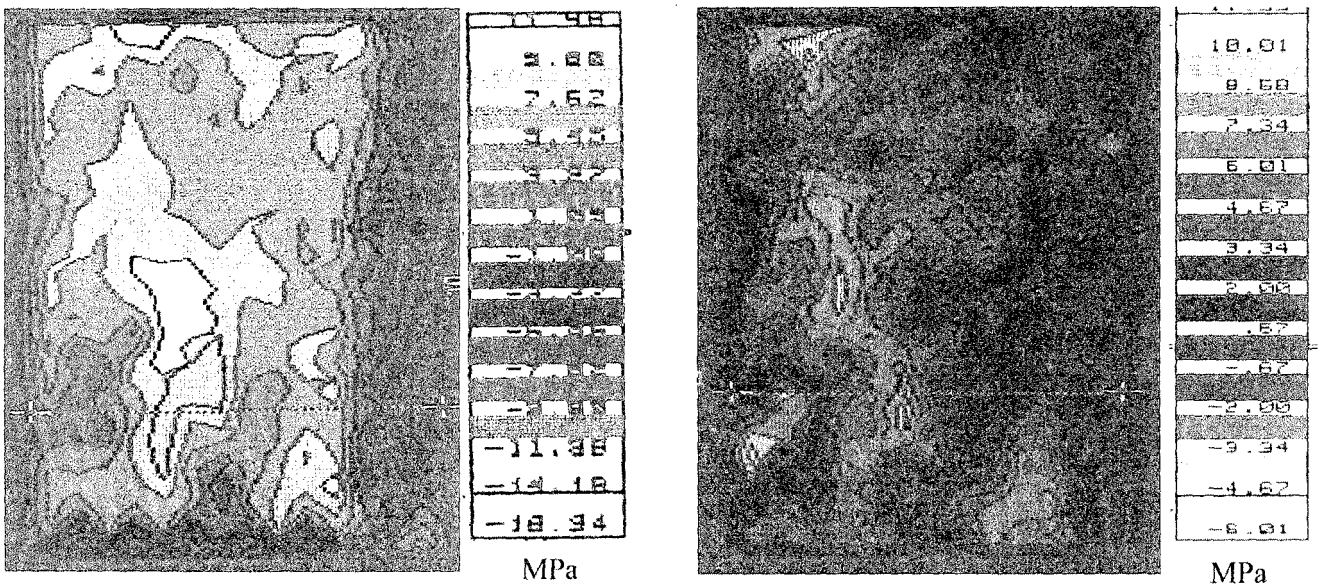

0.10×10^5 load cycles 1.02×10^6 load cycles

Figure 6: Initial SPATE scan I3F01 (left) and last SPATE scan I3F15 (right) both showing the presence of damage

Fig. 7 shows two of the 10 scans that were obtained from the front surface of specimen I1 using SPATE. The specimen was loaded at mean, amplitude and maximum stresses of 36.87 MPa, 15.38 MPa and 52.25 MPa, respectively and was cycles at 10 Hz. The two scans shown in Fig. 5 exhibited the two phenomena of internal and surface damage. This was seen from the fact that a lot of areas in the left scan in the figure had signals that were greater than the imposed load amplitude, while most of the areas in the right scan in the figure had signals that were less than the imposed load amplitude. The implication here was that of initial internal damage whose significance relative to the surface damage diminishes with the increasing number of load cycles.

The specimen front surface scans showed inwards and outwards spread of damage, starting from the edge and surface sites of initial damage. Consecutive SPATE scans that were obtained from the front surface showed an increase in the severity of damage and a spread of the damage with the number of load cycles. Thus, for instance, the area marked A covered with a yellow (white on the grey scale scans) hue on the top left of the left scan, showed a decrease in the magnitude of the recorded signal and a spread away from

the left edge, with continued cycling of the specimen.

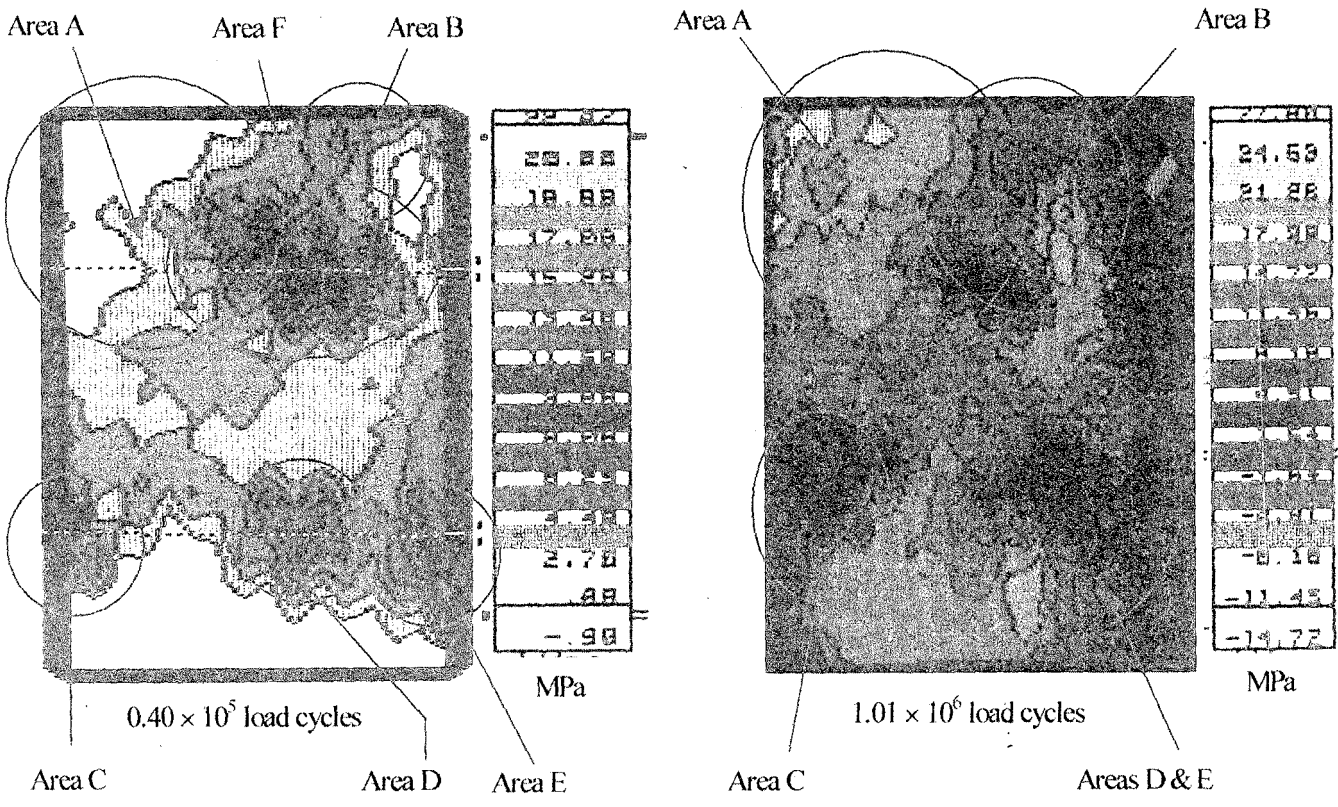

Figure 7: Initial SPATE scan I1F01 (left) and last SPATE scan I1F10 (right) both showing the presence of damage

The signal range in this area was observed to change from 20.00 MPa to 22.87 MPa at 0.40×10^5 cycles and 17.94 MPa to 19.81 MPa at 1.46×10^5 cycles, 14.88 MPa to 19.19 MPa at 6.16×10^5 cycles to 11.45 MPa to 14.74 MPa at 9.41×10^5 cycles. The area marked B on the top right corner of the left scan, also showed a decrease in the magnitude of the recorded signal, as well as a downward spread with increasing number of load cycles. The increase in intensity in this area was evident in the change of stress from the range 17.08 MPa to 18.88 MPa in the left scan, down to the range 11.46 MPa to 14.72 MPa in the right scan. The other centres of damage on the specimen marked C, D, E and F also exhibited similar trends. Damage in area C grew from initial values in the range 3.88 MPa to 11.68 MPa at 0.4×10^5 cycles to the values in the range –4.81 MPa to –1.84 MPa at 1.10×10^6 cycles. The spread of damage in the two damage centres marked,

D and E, eventually lead to their merging into one bigger area. The intensity of damage in these two areas increased with initial stresses in the range of 11.68 MPa to 13.48 MPa at 0.4×10^5 cycles to final stresses in the range of 4.51 MPa to 8.18 MPa at 1.10×10^6 cycles. The final level of the signal from the edge centres of damage was in the range -11.45 MPa to –8.18 MPa in comparison to the range 1.64 MPa to 4.51 MPa for most of the surface sites of damage. Given the fact that the severity of damage in both the surface as well as edge centres of damage was at the same level initially, the conclusion was reached therefore, that the edge centres of damage experienced the more rapid increase in the severity of damage of the two. The rest of the specimen surface other than at the centres of damage marked out in Fig. 7 showed little increase in the severity and spread of damage.

SPATE scans for the rear surface of specimen I1, two of which are shown in Fig. 8, exhibited sites of initial surface well as edge damage. The level of damage over most of the scanned rear surface was much higher than on the front surface, with initial surface internal damage signal-amplitudes reaching up to the range 38.55 MPa to 43.04 MPa. The front surface scans shown in Fig. 7 had much lower signals in the range 20.00 MPa to 22.02 MPa. The minimum signal on the rear surface was much lower than on the front surface being in the range -8.30 MPa to –5.50 MPa compared to a range between 8.08 MPa to 9.88 MPa for the front surface. The surface and edge centres of damage on the rear surface had signal amplitudes that were in the ranges –9.58 MPa to –6.76 MPa and 5.75 MPa to 8.68 MPa, respectively, at 1.31×10^5 cycles (3^{rd} scan). The equivalent values at 4.56×10^5 cycles (3^{rd} scan) for the front surface scans were 6.18 MPa to 7.22 MPa and 3.10 MPa to 6.18 MPa. This points to a higher severity of damage during the third scan, at both the surface and edge centres of damage on the rear surface, than on the front surface. Most of the rear surface had signals that were below 15.06 MPa at 9.96×10^5 cycles, compared to equivalent areas on the front surface, which has signals whose magnitudes were below 21.28 MPa at 1.01×10^6 cycles. This in addition to the fact that the initial signals were higher on the rear surface implies that surface damage accumulated much faster on the rear surface than on the front surface of the specimen. The presence of internal damage on both surfaces was evident from the fact that the initial SPATE signals on both surfaces had amplitudes that were much higher than the

imposed stress amplitude. The difference between the initial signals on both surfaces was likely to have been a result of different intensities of surface damage on the same through sections despite there being a similar effect on both surfaces, of the presence of internal damage. The differences could also have been partly due to different surface emmissivities as a result of differing matt black, hand spray coatings on the two surfaces.

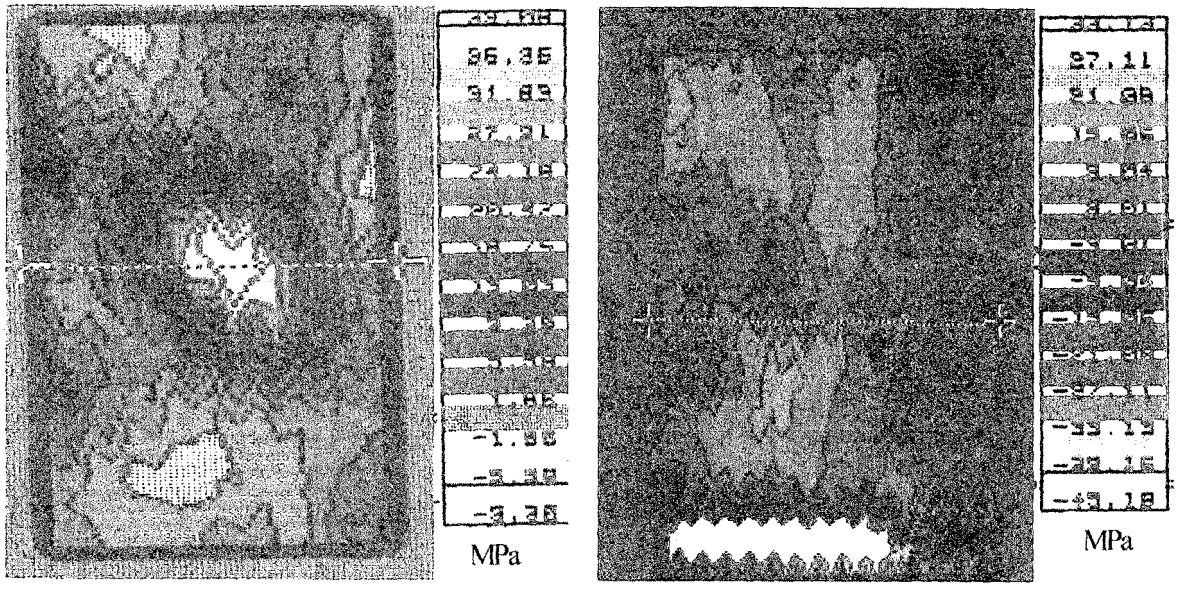

Figure 8: Second SPATE scan I1R02 (left) and last SPATE scan I1R10 (right) both showing the presence of damage

As was the case for the front surface scans, damage on the rear surface was seen to spread from the centres of initial damage and was higher in severity at the surface centres of initial damage than at the edge centres of initial damage up till the sixth scan. At this point the lower scanned edge experienced a very large signal reversal of up to –68.23 MPa that persisted at levels of up to –45.18 MPa till the last scan taken, the 10^{th} scan. It is important to note here that the lower scanned edge was very far from the clamp area as it was still within the gauge length. While the large signal reversal could have been due to bending effects, it could also have been due to fatigue failure setting in at this stage in the load history of the specimen.

Specimen I2 was loaded at mean, amplitude and maximum stresses of 36.87 MPa,

17.95 MPa and 54.82 MPa, respectively, and was cycled at 20 Hz. The SPATE scans for specimen I2, two of which are shown in Fig. 9, exhibited bulk damage that was not as severe as that shown by the other SPATE scans that have been discussed so far. Thus the amplitude of the measured signal remained within the range 8.01 MPa to 17.85 MPa for most of the test life of the specimen, dropping down to the range 8.19 MPa to 11.24 MPa at 7.38×10^5 cycles. A further but more drastic drop to the range -2.11 MPa to 2.11 MPa occurred at 7.63×10^5 cycles. Damage was seen to spread inwards and outwards from those sites, both on the edges and on the surface that had higher initial levels of damage, into the surrounding areas. Signal reversal in this specimen was very severe, with a minimum signal-amplitude in the range -22.28 MPa to -18.02 MPa and -40.03 MPa to -34.70 MPa at 0.11×10^5 cycles and 5.25×10^5 cycles respectively.

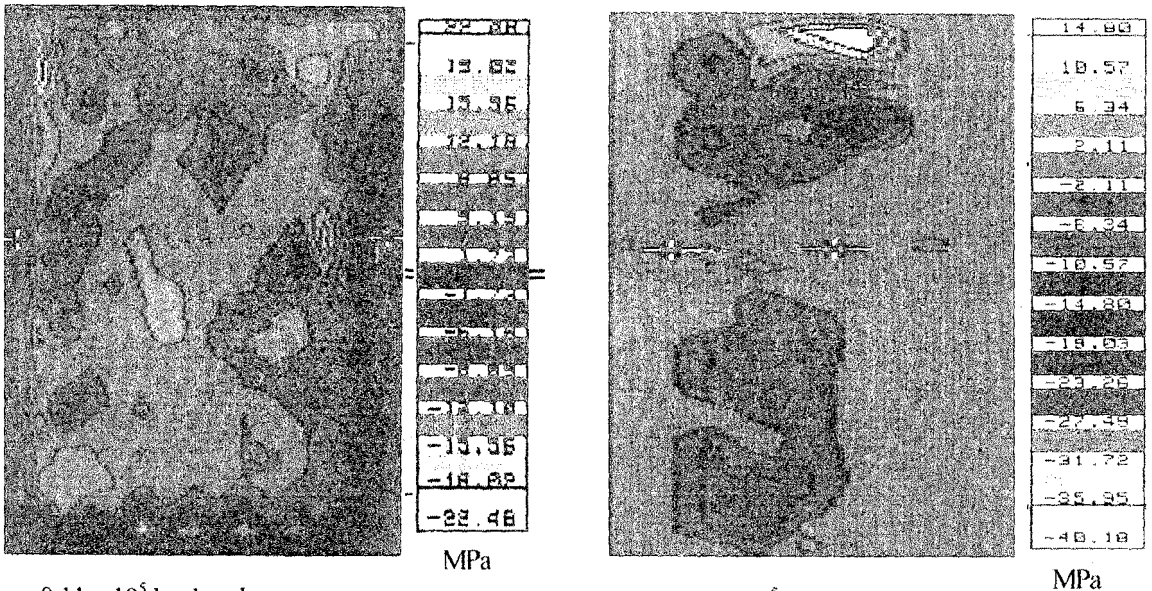

0.11×10^5 load cycles

7.63×10^5 load cycles

Figure 9: Initial SPATE scan I2F01 (left) and last SPATE scan I2F13 (right) both showing the presence of damage

Two of the six, SPATE scans for specimen A2, which was loaded at mean, amplitude and maximum stresses of 36.87 MPa, 17.95 MPa and 54.82 MPa, respectively, and which was cycled at 20Hz, are shown in Fig. 10. The SPATE scans for specimen A2 showed better conformity with the rest of the scans that have been discussed here unlike

the scans for specimen I2. The bulk and localised damage in specimen A2 were both higher in intensity very early in the test life of this specimen, relative to the other specimens that have been discussed so far, with initial signal amplitudes that were in the range 7.34 MPa to 9.42 MPa at 0.09×10^5 cycles. The amplitude of this signal decreased in magnitude at an increasing rate down to the range 1.75 MPa to 2.28 MPa at 3.38×10^5 cycles. Signal reversal occurred in localised spots early in the test life of the specimen, with initial signal amplitudes of -1.14 MPa to -5.27 MPa and -8.60 MPa to -7.06 MPa, at 0.09×10^5 cycles and 0.64×10^5 cycles, respectively.

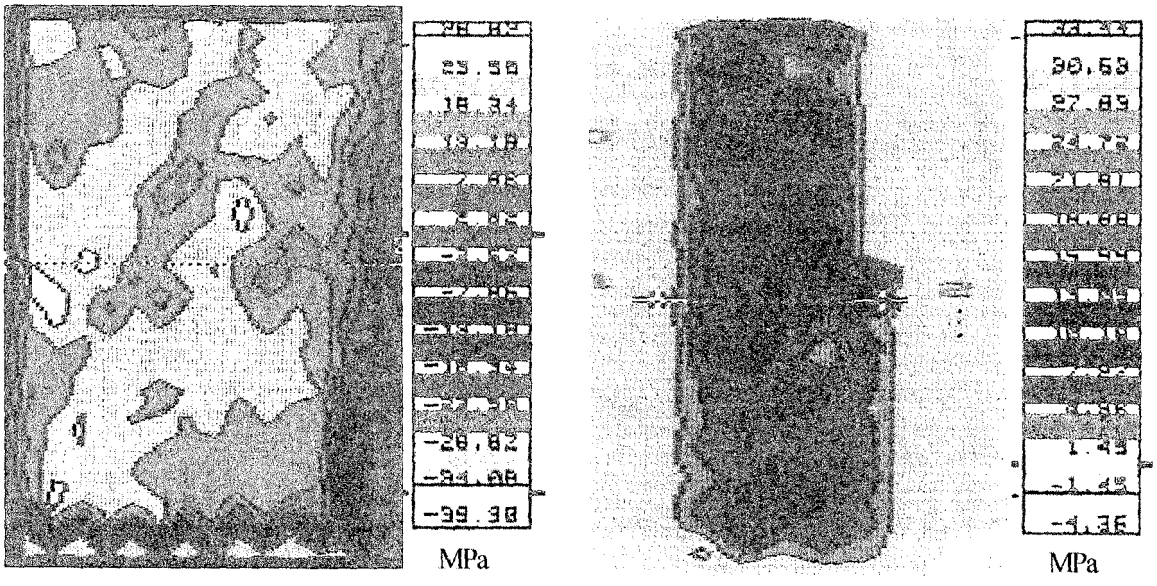

Figure 10: Initial SPATE scan A2F01 (left) and last SPATE scan A2F06 (right) both showing the presence of damage

7.0 DISCUSSION

As has been stated earlier, SPATE scans obtained from the surface of a homogenous material with no heat generating mechanisms of failure are expected to be of one uniform colour, coinciding with the colour code for the applied stress amplitude. The presence of different colours on the SPATE scans obtained here therefore, indicated the presence of material heterogeneity with its attendant heterogeneous coefficients of linear thermal

expansion, as well the existence of heat generating damage mechanisms. Occurrence of heat generating mechanisms in specimens that are loaded in cyclic tension-tension, it has been noted, leads to a reversal of the thermoelastic signal, while external and internal sites of stress concentration give rise to respective decreases and increases in the magnitude of the recorded signals. The characteristics of a SPATE scan obtained from a cycled specimen can therefore, be used to make inferences about its state.

The initial SPATE scans obtained from each specimen indicated that different levels of damage were present in the tested specimens even before testing began. This deduction was a result of the observed presence of signal reversal in the initial scans obtained. Initial damage was likely to have arisen during fabrication of the SMC sheets, occurring in the form of voids and flaws, and could also have been introduced during handling and cutting out of the test specimens. It is significant in this respect that all the specimens did show some initial edge damage. Damage, however, did also initiate during the course of testing. The spread and growth of damage was seen to stem from both the sites of existing initial damage and from those sites where damage was initiated during testing. SPATE scan C4FR01 and A4R01 of Fig. 4, with both edge and surface damage, are good examples of test specimens that exhibited initial damage.

Potter and Wong (1994), showed that temperature diffusion averaging between a fibre and the adjacent matrix, occurred at frequencies in the order of 10^{-5}s, which being so much lower than the normal SPATE scanning frequencies, obviated the effect of local heterogeneity between a fibre and the surrounding matrix. The magnitude of the signal for the SPATE scans of the SMCR26 that were carried out in the present work did however, exhibit a spatial variation, even at low stress levels where little damage was expected to occur. This is in contrast to the relatively smoother signals that are obtained for homogenous materials like steel and aluminium. The work of Dwyer (1993), showed the thermoelastic signal obtained from the surface of SMCR27 specimens to be higher in resin rich areas and lower in areas where the glass fibre content was higher, as a result of the differing thermoelastic constants for the constituent components. Clearly, therefore, the variation in the magnitudes of the thermoelastic signal obtained from the SMCR26 specimens prior to the onset of damage, (see Fig. 4), were an indication that the sources

of material heterogeneity were greater in size than the SPATE spatial resolution of 0.5 mm diameter.

It was not possible to identify any relationship between the stress amplitude and the spread of damage as well as accumulation of damage by inspection of any of the SPATE scans obtained. The scans however, did highlight the presence of initial damage, as well as the spread and accumulation of damage centred on the initial and cycling centres of damage. The identified centres of damage did not conform to any pattern and were located randomly, possibly as a result of the heterogeneous nature of SMCR26 and of the accumulation, as well as the spread of damage. The possibility of a frequency dependency of the accumulation of damage is raised by the results of the two specimens I1 and I3, which were tested under the same stress regimes, and at different frequencies. Specimen I3, which was tested at 20Hz, showed a more widespread and more severe level of initial bulk damage than specimen I1, which was tested at 10Hz. This possibility however, can only be confirmed from a much larger database than that obtained from the two specimens tested here alone.

Damage in a material can be quantified by observing the change in the magnitude of one or more of the macroscopic properties of the material. Taking for instance the onset of damage to be signified by a reduction in the magnitude of the measured thermoelastic signal below 10% of the amplitude of the thermoelastic signal that is obtained from the undamaged areas of the specimen. Further, taking a reduction in the magnitude of the measured thermoelastic signal below 50% of the amplitude of the thermoelastic signal that is obtained from the undamaged areas of the specimen, to imply the presence of significant damage, has three implications. First, that all the initial specimen scans that were exposed to the constant mean stress test regime, with the exception of the front and rear scans of specimen I1, showed significant edge damage. Secondly, that all the initial specimen scans exhibited the onset of damage. Third, that all the initial scans showed significant damage. The growth and spread of damage in subsequent scans was centred on the sites of initial damage and on the centres of damage developed as a result of cycling.

Based on the 10% and 50% limits taken arbitrarily to indicate the onset of and significant levels of damage in the previous section, significant damage on the surface

and edges was exhibited by all the initial specimen SPATE scans, under the constant stress-amplitude test regime. In almost all the cases, a significant proportion of the scanned areas of the specimens showed damage that was at and above the 10% level. Damage at and above the 50% level was only present in isolated patches. The extent of the areas that exhibited these two levels of damage varied randomly from specimen to specimen, without any relation to the stress amplitude or maximum stress.

8.0 CONCLUSIONS

- The foregoing work shows thermoelastic stress analysis to be a powerful method for detecting the presence of damage and for monitoring it's spread and increase in intensity.
- By comparing the initial SPATE scan with the subsequent scans that were obtained, it was possible to distinguish between the initial and cycling based centres of damage.
- Inspection of the numerous SPATE scans presented here did not identify any relationship between the spread of damage and the increase in the intensity of damage to the stress amplitude.
- The random manner in which the various centres of damage occurred on the scanned specimen surfaces and their random profiles were likely to be the result of the heterogeneous nature of SMCR26.
- The accumulation of damage was also heterogeneous in that it was seen to vary from one location to the other.

The effect of different mean stresses and constant stress amplitudes on the initiation and accumulation of damage form the subject of further research, the results of which will be published at a latter date.

9.0 ACKNOWLEDGEMENTS

Dr. S. Olutunde Oyadiji, of the School of Engineering, University of Manchester, UK, whose efforts and financial contribution helped greatly in the completion of this research. Dr. Janice Barton of the School of Ship Science, Southampton University, UK for her assistance. Dr. John Kihiu of the Department of Mechanical Engineering, JKUAT,

for taking time to peruse the original manuscript and for the numerous useful comments made thereafter.

REFERENCES

ASTM Standard E466, Practice For Constant Amplitude Axial Fatigue Testing of Metallic Materials, 03.01.

BS 3518: Part 1: 1993, Method of Testing: Fatigue - General principles.

Belgen M. H. (January 1967) Structural Stress Measurements with an Infrared Radiometer, *ISA Transactions*, **6**, 49 - 53.

Boyce B. R. (1991) TSA Signal Processing and Data Collection. Thermoelastic *Stress Analysis*, Edited by N. Harwood and Cummings W. M., lOP Publishing Ltd., pp. 71 - 79.

Dillon Jr. O. W. (1963) Coupled Thermoplasticity. *Journal of the Mechanics and Physics of Solids*, **11**, 21 - 33.

Dillon Jr. O. W. (1966) The Heat Generated During the Torsional Oscillation of Copper Tubes, International. *Journal of Solids and Structures*, **2**, 181-204.

Dulieu - Smith J. M. and Stanley P. (September 1994) Developments in the Interpretation of the Thermoelastic Response of Composite Materials. Experimental Techniques & Design in Composite Materials, 2nd International Seminar, 7 - 8 editor Found M. S., pp. 120 - 139.

Dulieu - Smith J. M. and Stanley P. (September 1996) A Review of Damage Studies in Fibre Reinforced Composites Using the Thermoelastic Technique. XXV AIAS National Conference, International Conference on Material Engineering, Gallipoli - Lecce, 4 - 7.

Dunn S. A., Lombardo D. and Sparrow J. G. (1989) The Mean Stress Effect in Metallic Alloys and Composites. *SPIE Proceedings of the International Conference on Stress & Vibration*, London, **1084**, 129 – 142.

Dwyer J. F, Dulieu - Smith J. M. and Stanley P. (1993) Predicting the Thermoelastic

Response and Relevant Material Properties of SMC. Proceedings of the Conference on Advances in Materials and Processing Technologies (AMPT '93), Dublin, 1613 – 1624.

Enke N. F. (1989) An Enhanced Theory for Thermographic stress Analysis of Isotropic Materials. *SPIE Proceedings of the International Conference on Stress and Vibration*: Recent Developments in Industrial Measurement and Analysis, **1084**, 85 – 102.

Everett G. M., Owens R. H. and Barker A. S. (1987) Developments in the Application of the Thermoelastic Technique to Structural Mechanics. *Proceedings of the 9th International Conference on Experimental Mechanics*, Copenhagen, Denmark, pp. 774-780.

Garroch C. (1996) Thermoelastic Assessment of Moulded Fibre Reinforced Composites. *Ph.D. Thesis, University Of Manchester.*

Harwood N., Cummings W. M. and MacKenzie A. K. (1991) *Introduction to Thermoelastic Stress Analysis*, Thermoelastic Harwood N and Cummings W. M., "Variable amplitude loading", Thermoelastic Stress Analysis, Edited by N. Harwood and Cummings W. M., IOP Publishing Ltd., pp. 85 - 103.

Harwood N and Cummings W. M. (1991) *Variable amplitude loading. Thermoelastic Stress Analysis,* Edited by N. Harwood and Cummings W. M., IOP Publishing Ltd., pp. 135 - 164.

Jones R., Heller M., Lombardo D., Dunn S., Paul J. and Sunders D. (1989) Thermoelastic Assessment of Damage Growth in Composites. *Journal of Composite Structures*, **12**, (4) 289 - 314.

Joule J. P. (1857) On the Thermal Effects of Longitudinal Compression of Solids. *Proceedings of the Royal Society*, 8, 355.

Liao K., Dunyak T. S., Wayne W., Stinchcomb W. W. and Reisfnider K. L. (May 6 – 7 1993) Monitoring Fatigue Damage Development in Ceramic Matrix Composite Tubular Specimens by a Thermoelastic Technique. *ASTM STP, 4th Symposium on Composite Materials: Fatigue and Fracture, Indianapolis,* **1156**, 620 – 636.

Machin A. S., Sparrow J. G. and Stimson M. G. (1987) The Thermoelastic Constant. *SPIE Proceedings of the 2nd International Conference on Stress Analysis by*

Thermoelastic Techniques, **23**, 27 – 30.

Machin A. S., Sparrow J. G. and Stimson M. G. (1987) Mean Stress Dependence of the Thermoelastic Constant. *Strain,* February, pp. 27-30.

Maringa M., (2002) Investigating the Mechanical Properties of Sheet Moulding Compound (SMCR26). Detecting Fatigue Damage and Monitoring Fatigue Damage Accumulation in the Material. *Ph.D. Thesis, University of Manchester, UK.*

Maringa M. and Oyadiji S. O. (November 2002) Use of Thermoelastic Measurements for the Detection of Damage and its Accumulation. *Proceedings of the 73rd Annual Shock and Vibration Symposium, Newport, Maryland, USA.*

Mckelvie J. and MacKenzie A. K. (1991) Signal Attenuation due to Internal and External Factors. *Thermoelastic Stress Analysis*, Edited by N. Harwood and Cummings W. M., lOP Publishing Ltd., pp. 85 - 103.

Mitrovic M. and Carman G. P. (1996) Effect of Fatigue in Woven Composites on Thermal-Mechanical Properties and Residual Compressive Strength. *Journal of Composite Materials,* 30, No. (2) 164 - 189.

Ometron User manuals, (1987). *SPATE / VPI Series 9000 Operator's Manuals Volumes 1 – 3*, Ometron Ltd.

Potter R. T. and Wong A. K. (7 - 8 September 1994) Thermoelastic Analysis of Composites, Experimental Techniques & Design in Composite Materials. *2nd International Seminar*, editor Found M. S., pp. 105 - 119.

Rocca R. and Bever M. B. (February 1950) The Thermoelastic Effect in iron and nickel as a Function of Temperature. Transactions of AIME, *Journal of Metals*, **188**, pp. 327 - 333.

Stanley P. and Chan W. K. (1988) The Application of Thermoelastic Stress Analysis Techniques to Composite Materials. *Journal of Strain Analysis,* **23**, (3), 137 - 143.

Stinchcomb W. W., Reifsnider L. A., Marcus L. A. and Williams R. S. (1975) Effects of Frequency on the Mechanical Response of two Composite Materials to Fatigue Loads, Fatigue of Composite Materials. *ASTM STP 569, American Society for Testing and Materials*, pp. 115 - 129.

Stress Photonics, http://www.stress.photonics.com, 2002.

Thomson W. (December 15 1851) On the Thermoelastic and Thermomagnetic Properties of Materials, *Transactions R. S. E.*, pp.57 - 77.

Wang S. S. and Chim E. S. - M. (March 1983) Fatigue Damage and Degradation in Random Short Fibre SMC Composite. *Journal of Composite Materials*, **17**, 114 – 134.

Weber W. (1830) Ueber Die Specifische Wärme fester Körper, insbesondere der Metallie, *Annalen der physik und chemie, jahrgang, zehntes stück*, pp. 177 – 213.

Wong A. K, Jones R. and Sparrow J. G. (1987) Thermoelastic Constant or Thermoelastic Parameter? *Journal of the Physics and Chemistry of Solids*, **48**, (8), 749 - 753.

Zhang D. and Sandor B. I. (1992) Advances in Thermographic Stress Analysis and Evaluation of Damage in Composites. *ASTM STP, Advances in Fatigue Lifetime Predictive Techniques, San Francisco*, **1120**, 428 - 443.

Zhang D. and Sandor B. I (1992) Damage Evaluation in Composite Materials Using Thermographic Stress Analysis. *ASTM STP Advances in Fatigue Lifetime Predictive Techniques, San Francisco,* **1122**, 341 – 353.